15th Meeting of the International
Collaboration on Advanced Neutron Sources
November 6-9, 2000, Tsukuba, Japan

22.2

Solid-State Ultra-Cold-Neutron Detectors

T.Kitagaki[1],M.Higuchi[2],K.Sakai[3],M.Utsuro[4],
M.Hino[4],P.Geltenbort[5] and J.Butterworth[5]

1 Neutrino Center, Tohoku University, Sendai 980-8578 Japan
2 Faculty of Engineering, Tohoku Gakuin University
3 Department of Physics, Tokyo Institute of Technology
4 Research Reactor Institute, Kyoto University
5 Institut Laue Langevin, Grenoble

Abstract

Solid state UCN detectors with ^{6}Li compound converters with a variety of critical velocity, 2.1 - 5.0 m/s, were tested at ILL. All detectors are usable as the UCN detectors. However, the detectors seemed to ignore their critical velocities. They measured Ultra Cold Neutrons down below their critical velocities without showing the cuts predicted by the elementary theory. This anomalous absorption of UCN is thought to be attributed to the micro-structure of the solid state converter layers.

Any substance has a Fermi potential, U, and corresponding critical velocity, V_c, for slow neutrons. It is the space diluted nuclear potential and given by the number density of atoms, ρ, and the average coherent scattering length per atom for the neutron scattering, b,

$$U = (\hbar^2/2m).4\pi\rho b \qquad (1)$$
$$V_c = (\hbar/m).(4\pi\rho b)^{1/2} \qquad (2)$$

U is typically 2.4x 10^{-7} eV and V_c is 6.8 m/s for nickel. The ultra cold neutrons (UCN) with the energy lower than such potential are totally reflected by the potential and can be stored in a vessel. On the other hand, this noble feature generally hampers the direct UCN detection, because neutrons with vertical incident velocities those are smaller than the critical velocity hardly come into the detector.

We have been developing a type of solid state UCN detector, [1], which measures the UCN directly without gravitational acceleration. This time, we prepared solid state detectors for a variety of critical velocities, 2.1 - 5.0 m/s, and tested them at ILL. This note presents the results of the test on the effect of critical velocity to the detector efficiency. The exploration of the absorption of UCN into the strongly absorptive converters will open a new way to investigate the interactions of UCN with solid matter.

Experiment and results

Our detector was originally designed for the direct measurement of UCN in a liquid helium cryostat. Therefore, it consists of all solid components, a thin converter film of ^6Li compound in a frame and a PIN silicon-diode which detects the produced t and α from the reaction $^6Li(n,\alpha)t$. The use in a cryostat requires it to be compact, simple and sturdy. Fig.1 shows our present standard unit, which consists of a thin converter target and a silicon-diode. The size of diode is 3.6 cm square and its sensitive area is 7.84 cm^2. The converter is easily replaced, and several units are used in parallel for the purpose.

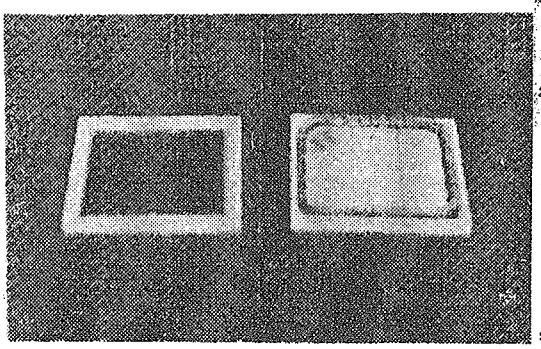

Figure 1. Detector
Left: Silicon diode, 3.6 cm square, and
Right: one set of detector;
converter and diode

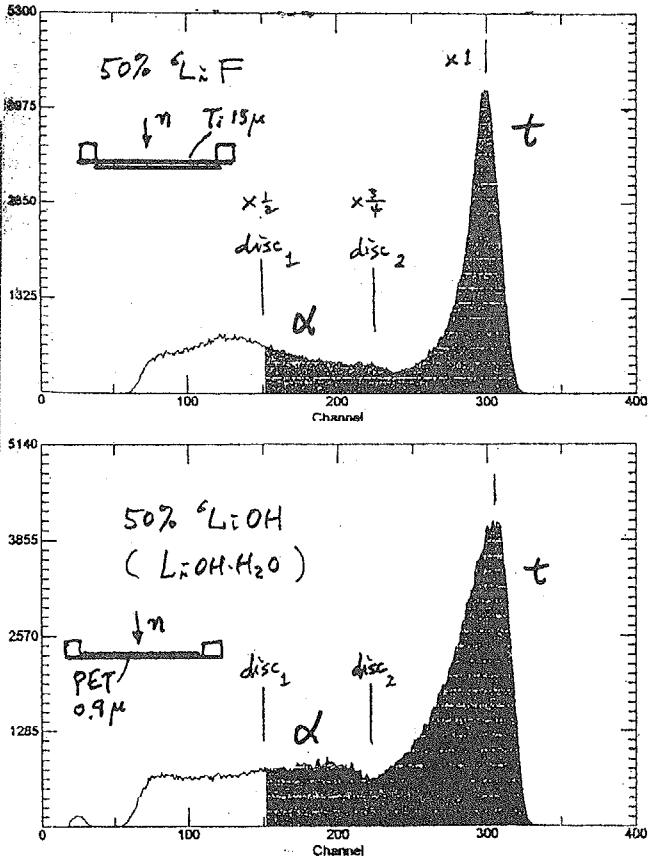

Figure 2. Pulse height distributions,
$n + ^6Li \rightarrow \alpha(2.05\text{MeV}) + t(2.73\text{MeV})$
(a) LiF and (b) $LiOH$

Two types of converter target were developed, $Ti - LiF$ and $LiOH - PET$. The LiF is evaporated on a titanium foil of 15 μm thickness, and the titanium foil faces the incident neutrons. The $LiOH$ is deposited on a PET foil of 0.9 μm thickness by the water solution method, and the $LiOH$ layer directly faces incident neutrons. Fig.2 (a) and (b) show their pulse height distributions, where the t and alpha peaks are seen. The discrimination level was set at 3/4 of the t peak position in the present test, i.e. mostly t's were measured in a 2π geometry. Our standard set of discrimination levels are however at 1/2, which is shaded in Fig.2. This is sufficient to discriminate the gamma tail from the lower side. The pre-amplifier is a charge sensitive amplifier.

Table 1 Converter targets, (* He cps = x1/2)

Abbre.	material	V_c m/s	UCN<7.5m/s cps	VCN>7.5 cps	VCN/UCN	Thermal n cps,arb
$9F$	$95\%^6LiF$	5.0	2.97	6.35	2.14	1.69
$5F$	$50\%^6LiF$	4.2	3.34	6.15	1.84	0.85
$9H$	$95\%^6LiOH$	2.9	2.67	4.67	1.74	1.18
$5H$	$50\%^6LiOH$	2.1	3.14	4.07	1.30	0.42
He	^3He counter	3.2(Al)	* 3.56	* 6.20	1.74	

Table I lists the converter targets used in the present measurement, $95\%^6LiF(9F)$, $50\%^6LiF(5F)$, $95\%^6LiOH(9H)$, and $50\%^6LiOH(5H)$, where the percentages denote the fraction of ^6Li in lithium. The fraction of ^6Li adjusts the critical velocity, V_c= 5.0, 4.2, 2.9 and 2.1 m/s respectively.

The measurement was made at the UCN test beam line of ILL during June and July, 2000. The UCN beam from the horizontal guide tube ($v > 3.2$ m/s) was bent 90 degrees and vertically transported by 0.90 m. The velocity of UCN at the detector were defined by the vertical time of flight method (TOF) in the top 0.50 m distance using a horizontal rotating chopper.

Before discussing the data, we briefly review what the elementary theory predicts for a strongly absorptive medium such as the present converter. For a potential, U,

$$[-(\hbar^2/2m)\Delta + U]\phi = E\phi \qquad (3)$$

$$k^2 = k_o^2 - 4\pi\rho b\ , \qquad (4)$$

where k_o is the wave number in vacuum and k is the complex wave number in the medium with strong absorption due to its complex scattering length,

$$b = b' - ib''\ . \qquad (5)$$

By the optical theorem, $b'' = k_o\sigma_t/4\pi \approx k_o\sigma_a/4\pi$, (6)

$$k^2 = k_o^2 - 4\pi\rho b' + i\rho k_o\sigma_a \ . \quad (7)$$

The surface transmission probability is given by

$$T(v) = 1 - |(k - k_o)/(k + k_o)|^2 \ . \quad (8)$$

The transmission probabilities, $T(v)$, for step function potentials are shown in Fig.7 (a) for $9F$, $5F$, $9H$ and $5H$ targets respectively. They have tails below the critical velocities due to the quantum penetration, although the amount of tail is small for the nominal absorption cross section and the cut feature is always clear at the critical velocities.

Fig.3 shows the velocity dependence of neutron counting of detectors with and without filters. (a) the $50\%^6LiF$ detector $(5F)$ with and without aluminum filter, (b) the same with and without nickel filter, and (d) and (e) are corresponding enlarged plots. The aluminum filter is made of two superimposed 20 μm thick foils, and the nickel filter is made of a 2000 Angstrome thick layer on a 15 μm thick aluminum backing foil. The curves, P, are the penetration probabilities of the filters, which are the ratio of two curves with and without a filter. They show the expected cuts of the filters at their critical velocities. The TOF resolution whose FWHM is shown by the horizontal bars shows the smearing of the observed cuts for nickel. However, the detector measured UCN below $V_c(Ni)$=6.8 m/s, and furthermore down below its critical velocity, $V_c(50\%^6LiF)$=4.2 m/s without showing the expected cut. This peculiar absorption of UCN in LiF was also observed in the reflection measurement of UCN from ^6LiF, [2], where the single crystal of LiF showed a cut at 5.1 m/s, nominal critical velocity of ^6LiF, and the evaporated LiF absorbed UCN down below 3 m/s. Figures, (c) and (f), are similar plots for the $50\%^6LiOH$ detector $(5H)$ with and without nickel filter. It also measured UCN below its critical velocity, $V_c(50\%^6LiOH)$ = 2.1 m/s.

Fig.4 compares detectors. (a) $5F$ and $9F$, (b) $5H$ and $9H$, (c) ^3He gas counter and $5F$, where the curves are normalized at 7.5 m/s to compare only the velocity dependences. The points, which are the ratios of two curves, show the relative efficiencies. It is clear that the 50% targets are more efficient than the 95% targets in the UCN region for both of LiF and $LiOH$, i.e. the lower the critical velocity, the larger the efficiency in the UCN region. A similar comparison of $5F$ and $9H$ shows that they have very simlar velocity dependences. Therefore, the efficiency for the UCN measurement and also the signal to noise ratio are larger in the inverse order of critical velocities.

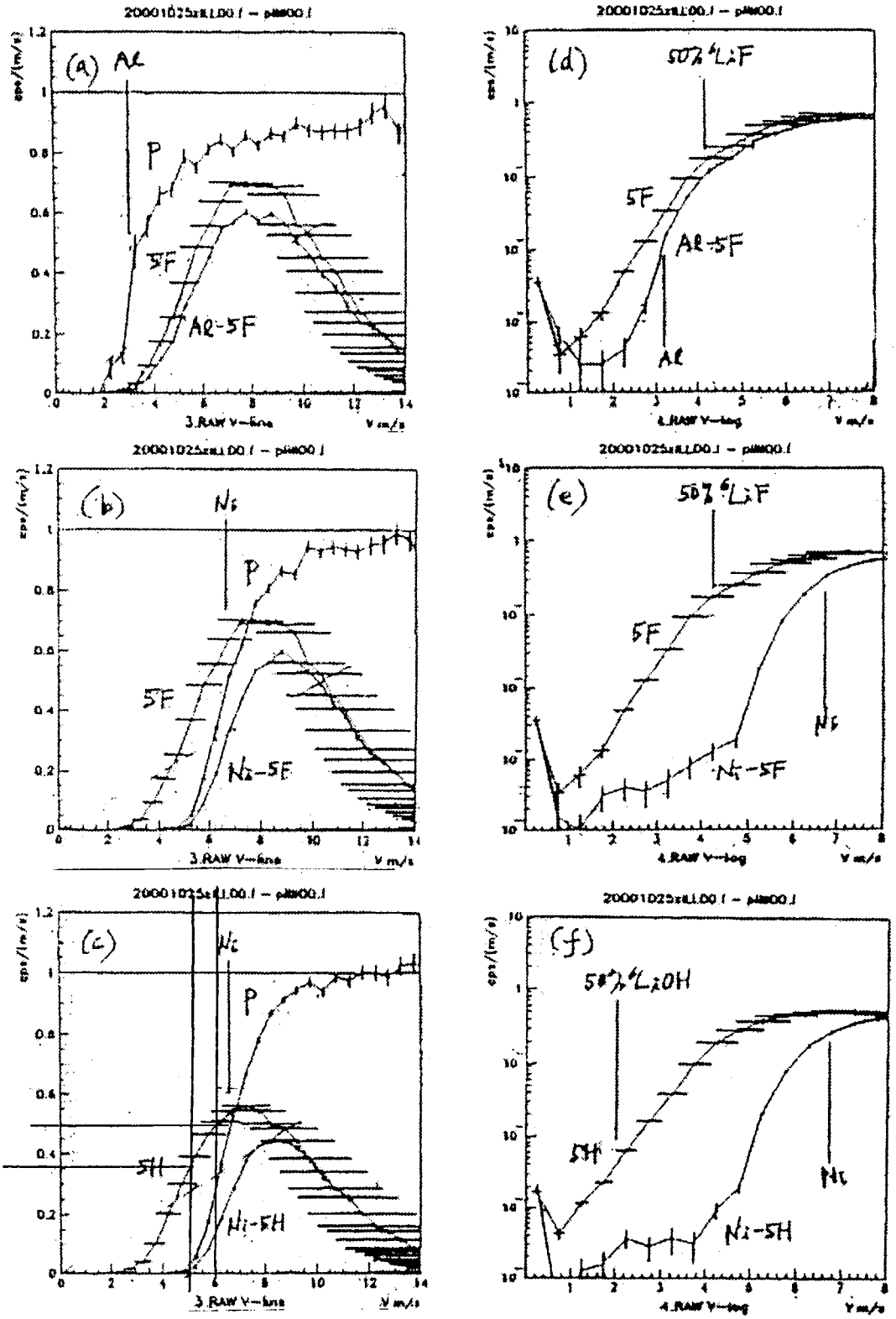

Figure.3 Velocity dependences of detectors with and without filter.
(a) $\mathbf{50\%^6LiF(5F)}$ and aluminum filter, (b) $\mathbf{5F}$ and nickel filter, and (c) $\mathbf{50\%^6LiOH(5H)}$ and nickel filter. The curves ,$\boldsymbol{P}$, are the penetration probabilities of filters. (d), (e) and (f) are enlarged plots respectively. The horizontal bars show the TOF resolution and the vertical bars critical velocities.

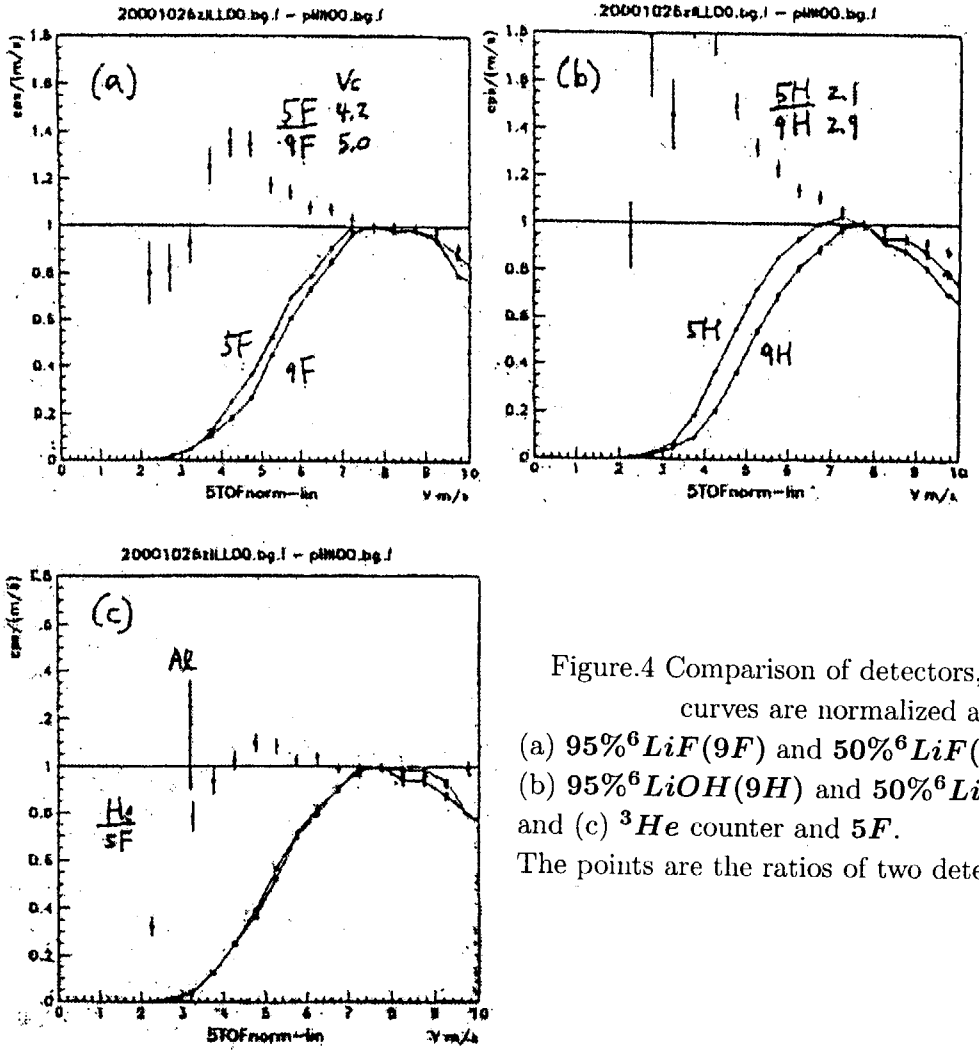

Figure.4 Comparison of detectors,
curves are normalized at 7.5 m/s.
(a) $95\%^6LiF(9F)$ and $50\%^6LiF(5F)$,
(b) $95\%^6LiOH(9H)$ and $50\%^6LiOH(5H)$,
and (c) ^3He counter and $5F$.
The points are the ratios of two detector curves.

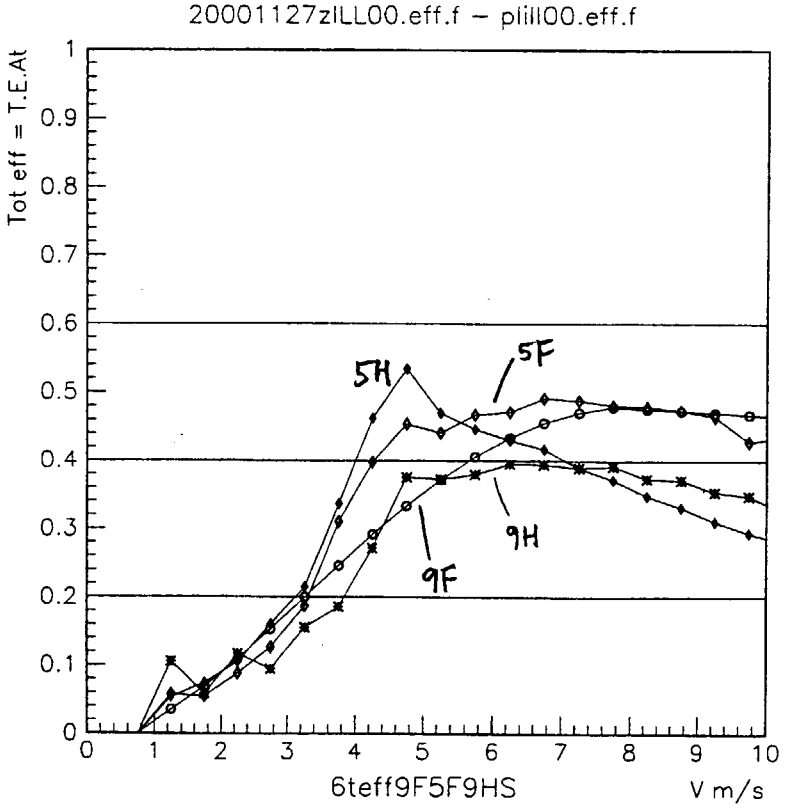

Figure.5 Neutron counting efficiencies of the detectors, $[T(v).\epsilon_{cap}(v)].\epsilon_{at}$, data.

$$9F < \left(\begin{array}{c} 5F \approx 9H \\ \approx He(> 3m/s) \end{array} \right) < 5H. \qquad (9)$$

We tested a ^3He gas counter in the same beam condition as a comparison. It is a standard flat ^3He counter with a diameter of 10 cm and 100 micron thick aluminum window, and we measured only the $(p+t)$ peak in a 4π geometry. Figure (c) compares the helium counter and $5F$ detector. Their velocity dependences are very close above the aluminum cut, however, the absolute count of the helium counter (per 7.84 cm^2) is about twice of that of the $5F$ detector, (Table I), because of the difference of 4π and 2π detections.

The neutron count of detector is generally given by

$$C(v) = \Phi(v).[T(v).\epsilon_{cap}(v)].\epsilon_{\alpha t} \qquad (10)$$

Φ is the neutron flux and $\epsilon_{\alpha t}$ is the counting efficiency of detector for produced α and t, which is approximately a constant for each detector. Therefore, the velocity dependence of the detector is in $[T(v).\epsilon_{cap}(v)]$, the interaction probability per neutron, where T is the surface transmission probability into the target. In the case of $Ti - LiF$ converters, the titanium foil penetration, $P_{Ti}(v)$, is included in T. ϵ_{cap} is the absorption probability of neutrons in the target layer by the ^6Li nuclear interactions and given by

$$\epsilon_{cap}(v) = 1 - exp(-\sigma_a(v').N_a.x) \qquad (11)$$

$$= \sigma_{th}.N_a.x \quad \text{for thermal neutrons} \qquad (12)$$

$$\sigma_a(v') = \sigma_{th}.v_{th}/v' \ , \qquad (13)$$

N_a is the ^6Li atom density, σ_a the absorption cross section, v' the velocity in the matter, and the subscript, th, denotes thermal neutrons. ϵ_{cap} has a peak at the critical velocity and decreases exponentially towards thermal velocity. Table I summarizes the result, where the thermal neutron counts are proportional to the amount of ^6Li, (eq.12). Since the thickness of targets were approximately adjusted to be the same for each of LiF and $LiOH$, the amount of ^6Li shows wide spread which is proprtional to the fraction of ^6Li in lithium. However, the UCN counts (<7.5 m/s) are not much different from each other in spite of the large spread of the thermal neutron counts, because the critical velocities of detectors are in the UCN region and the absorption cross section increases divergently at the critical velocitiy. For the present conveter thickness, the $\epsilon_{cap}(v)$ is less than 0.015 for thermal neutrons, therefore, a good signal to noise ratio for UCN measurement is

guaranteed. In the present 50% ^{6}LiF target, the amount of ^{6}Li is about 0.074 mg/cm^2.

Fig.5 shows the neutron counting efficiencies of the detectors (counts per neutron), $[T(v).\epsilon_{cap}(v)].\epsilon_{at}$, obtained from the data. The neutron flux was estimated from the $9F$ data by applying a) the measured titanium-foil penetration, b) the surface transmission obtained from the Bates's data, [2] , c) the calculated $\epsilon_{cap}(v)$, and d) ϵ_{at} obtained by a simulation. The neutron counting efficiencies are about 0.45 per neutron for the $5F$ and $5H$ detectors at 5 - 6 m/s and 0.2 at 3.2 m/s with our standard discrimination level. Fig.5 shows what we have seen in raw data more quantitatively. The $5H$ detector measures UCN more efficiently than the $9F$ detector. However it does not reflect its critical velocity, 2.1 m/s, directly.

Discussion

We have seen that the velocity dependences of present detectors did not follow the prediction of simple elementary theory. It is thought to be due to the micro structure of converter layers. Fig.6 (a) and (b) show the surface of the 95% ^{6}LiF converter layer viewed by secondary-emission electron microscopy. The evaporated layer is divided into islands of tens micron size by many cracks, and the outline of islands are irregular and their surface is not perfectly flat. They are not large single crystals but large pieces of dried mud of micro crystals, much smaller than 0.1 μm which is the wave length of 4 m/s UCN. It was reported that the evaporated LiF layer was full of micro voids and the voids occupied 30% of volume.[3] Fig.6 (c) and (d) are similar pictures of the surface of the 95%$^{6}LiOH$ converter layer made by the water solution method. It is an aggregation of large crystal flakes of few/several μm size with a thickness of 0.1 - 0.2 μm. The crystal flakes stand randomly and the surface is full of caves and valleys.

Thus, the present target layers are rough and porous. The micro voids (smaller than the neutron wave length) especially in LiF will dilute the density and reduce the height of potential, U. They will also smooth out the shape of the potential at the surface from the step function. Both of these facts reduce the reflection and increase the absorption, and the effect is phenomenologically represented by one parameter, the enhancement of absorption cross section, $\sigma_a \rightarrow \chi_\sigma \sigma_a$. The macro (larger than the neutron wave length) cave can trap UCN as in a micro-UCN-bottle. This also increases the absorption and the effect is included in the above χ_σ. Even for a finely treated copper wall for the UCN storage, it was reported that an artificial

increase of χ_σ by 2.6 could describe the reflection loss of UCN, [4].
Fig.7 (a) is T, the surface transmission predicted by the theory, (eq.8), and (b) is $[T(v).\epsilon_{cap}(v)]$, which includes the absorption in the target, slightly shifted from (a). A large χ_σ enhances the T especially below the critical velocity. As can be seen in Fig.7 (c) for χ_σ of 15, the $9F$ transmission curve is enhanced close to the Bates data, [2], which is shown by the solid curve in the figure.

On the other hand, the macro size planes covering the surface with random directions in $LiOH$,(Fig.6 (d)), will give large incident angles for neutrons, which effectively stretches the T curve towards large velocity. For this effect, we introduce the incident-angle spread parameter, θ_{in}. Fig.7 (d) shows the T curves for the isotropic incident-angle distribution limited below θ_{in}= 45 degrees, where the curves are stretched and the heights are completely suppressed at their critical velocities.

The modified efficiencies by just one of parameters, $9F$ in (c) and $5H$ in (d), reproduce those of $9F$ and $5H$ in Fig.5 well. Therefore, we conclude that the observed peculiar behavior of velocity dependence is attributed to the micro structure of the solid state targets and the two parameters can represent the rough structure.

Conclusions

All tested detectors measured UCN down below their nominal critical velocities with nice signal to noise ratios. They all can be used for the direct UCN measurement. Their velocity dependences are not much different from each other despite of the spread of critical velocities because they apparently ignore their critical velocities. The total counting efficiencies of the detectors, $[T(v).\epsilon_{cap}(v)].\epsilon_{at}$, are approximately 0.45 per neutron at 5-6 m/s and falls off below 3 m/s for $9F$, $5F$ and $5H$, Fig.5. However, more detailed investigation in the comparison of the normalized velocity dependences shows that the lower the critical velocity, the larger the UCN efficiency. The $50\%^6LiOH(5H)$ is the best among the tested ones for general use, and the $50\%^6LiF(5F)$ detector might be the best for use in a liquid helium cryostat.

The anomalous absorption of UCN observed in the present detectors, apparently ignoring of their critical velocityies, is qualitatively understood as an effect of the porous structure of the converter layers. It suggests a direction for further improvement, for example, in detectors with much higher sensitivity below 3 m/s.

References

[1] T.Kitagaki, et al.,Int.Sym.on Neutron Optics, Kumatori (1996), J.Phys.Soc.Jpn.65 (1996) Suppl.A 163
[2] J.C.Bates, Nucl.Inst.Meth.150 (1978) 261
[3] L.G.Schulz, J.Chem.Phys.17 (1949) 1153
[4] L.V.Groshev et al.,JINR Comm R3-9534 Dubna (1976), See A.Steyerl, Neutron Physics (1977) 98

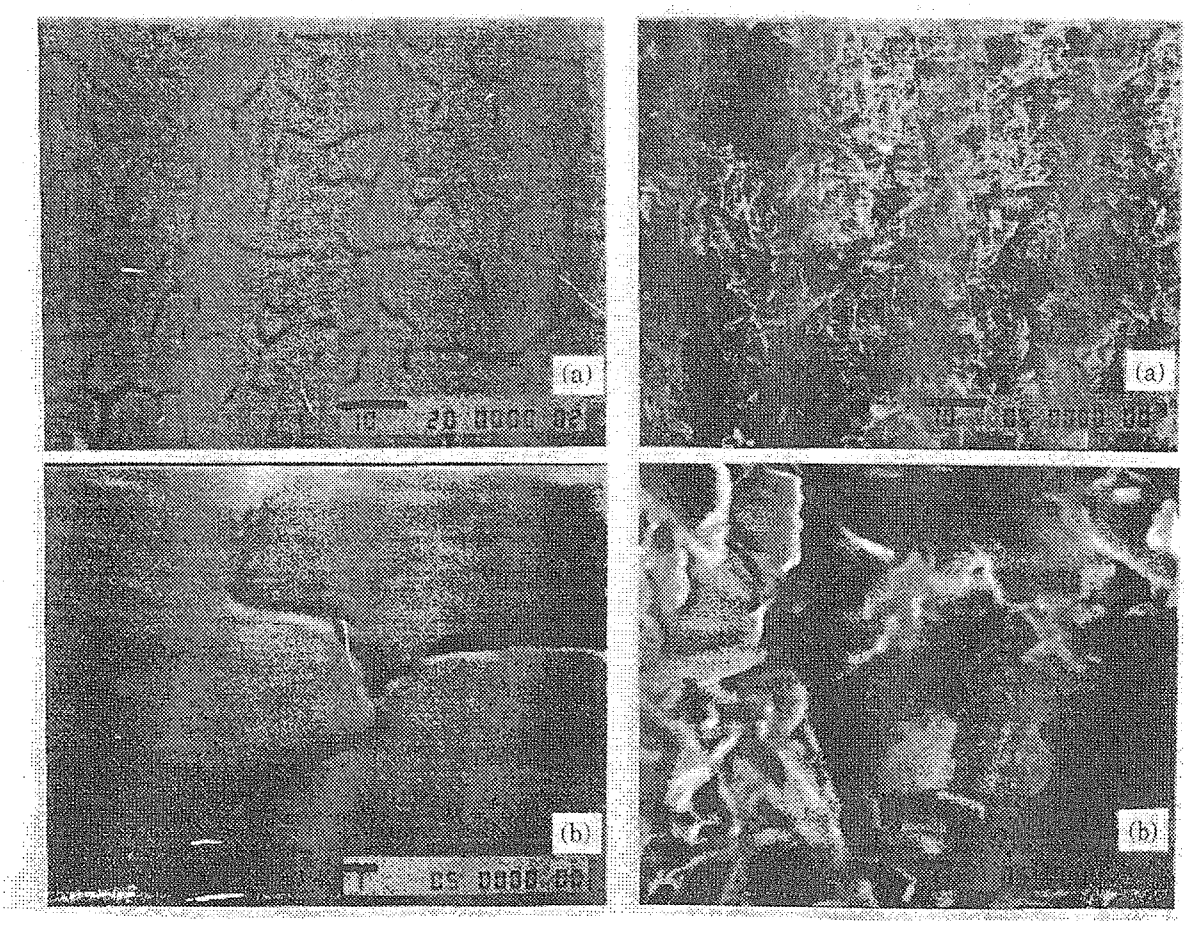

Figure 6. Surfaces of the converter layers viewed by Secondary-emission Electron Microscopy
(a) and (b) are ***LiF*** converter, and (c) and (d) ***LiOH*** converter. Magnification: (a) and (c) x1500, and (b) and (d) x7500. The horizontal bars are the scales in microns.

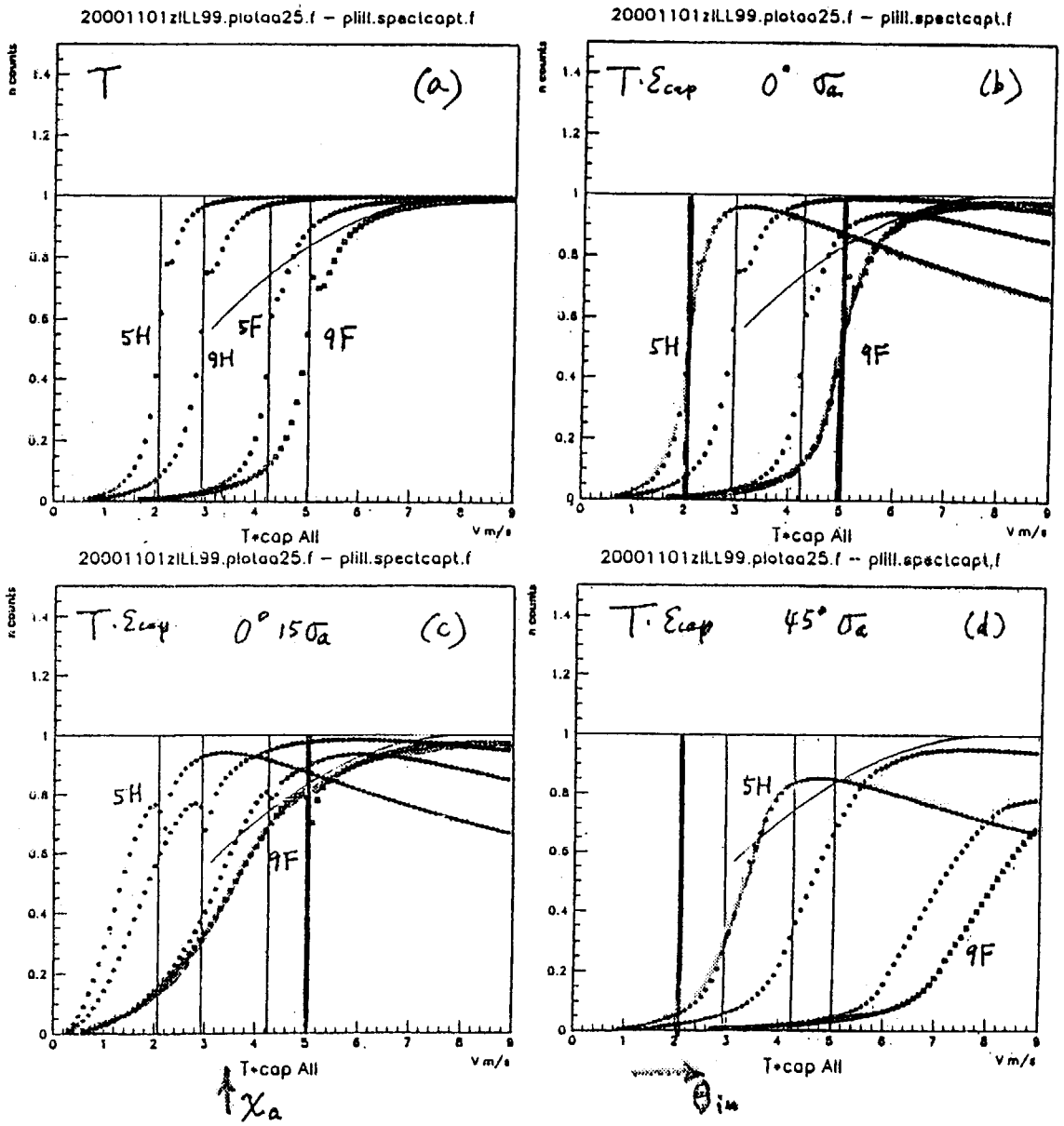

Figure 7. Efficiency of detectors, calculation.
(a) Transmission curves, T, by the elementary theory for $95\%^6LiF(9F)$, $50\%^6LiF(5F)$, $95\%^6LiOH(9H)$, and $50\%^6LiOH(5H)$ respectively.
(b) $[T(v).\epsilon_{cap}(v)]$ including the absorption in targets.
(c) With an absorption parameter, $\chi_\sigma = 15$.
(d) With an incident angle parameter, $\theta_{in} = 45$ degrees.